Low-Density Hyper-Confined Molecular Hybrids: Multifunctional Design and Mechanical Behavior

Reinhold Dauskardt
LELAND STANFORD JUNIOR UNIVERSITY

04/01/2020
Final Report

REPORT DOCUMENTATION PAGE

Form Approved
OMB No. 0704-0188

The public reporting burden for this collection of information is estimated to average 1 hour per response, including the time for reviewing instructions, searching existing data sources, gathering and maintaining the data needed, and completing and reviewing the collection of information. Send comments regarding this burden estimate or any other aspect of this collection of information, including suggestions for reducing the burden, to Department of Defense, Executive Services, Directorate (0704-0188). Respondents should be aware that notwithstanding any other provision of law, no person shall be subject to any penalty for failing to comply with a collection of information if it does not display a currently valid OMB control number.
PLEASE DO NOT RETURN YOUR FORM TO THE ABOVE ORGANIZATION.

1. REPORT DATE *(DD-MM-YYYY)* 29-06-2020	2. REPORT TYPE Final Performance	3. DATES COVERED *(From - To)* 15 Sep 2016 to 14 Sep 2019

4. TITLE AND SUBTITLE		
Low-Density Hyper-Confined Molecular Hybrids: Multifunctional Design and Mechanical Behavior	**5a. CONTRACT NUMBER**	
	5b. GRANT NUMBER FA9550-16-1-0354	
	5c. PROGRAM ELEMENT NUMBER 61102F	
6. AUTHOR(S) Reinhold Dauskardt	**5d. PROJECT NUMBER**	
	5e. TASK NUMBER	
	5f. WORK UNIT NUMBER	

7. PERFORMING ORGANIZATION NAME(S) AND ADDRESS(ES) LELAND STANFORD JUNIOR UNIVERSITY 450 SERRA MALL STANFORD, CA 94305-2004 US	8. PERFORMING ORGANIZATION REPORT NUMBER

9. SPONSORING/MONITORING AGENCY NAME(S) AND ADDRESS(ES) AF Office of Scientific Research 875 N. Randolph St. Room 3112 Arlington, VA 22203	10. SPONSOR/MONITOR'S ACRONYM(S) AFRL/AFOSR RTA1
	11. SPONSOR/MONITOR'S REPORT NUMBER(S) AFRL-AFOSR-VA-TR-2020-0073

12. DISTRIBUTION/AVAILABILITY STATEMENT
A DISTRIBUTION UNLIMITED: PB Public Release

13. SUPPLEMENTARY NOTES

14. ABSTRACT
Our project focuses on low-density hybrid nanocomposites where polymers are confined at molecular length scales in a nanoporous matrix. Our goal is to develop a fundamental understanding of the effects of hyper-confinement in low-density hybrids, which provides guidelines for exploring the limits of strengthening and toughening to create mechanically robust hybrids for aerospace applications. We also exploit the opportunity of creating high-temperature low-density hybrids for aerospace applications by the combination of high-temperature low-density hybrid nanoporous matrix together with polyimides with superior temperature capabilities.

15. SUBJECT TERMS
hybrid materials, hyper-confined molecules, materials toughening, high temperature polyimides

16. SECURITY CLASSIFICATION OF:			17. LIMITATION OF ABSTRACT	18. NUMBER OF PAGES	19a. NAME OF RESPONSIBLE PERSON PAN, MING-JEN
a. REPORT Unclassified	b. ABSTRACT Unclassified	c. THIS PAGE Unclassified	UU		19b. TELEPHONE NUMBER *(Include area code)* 703-696-7343

Standard Form 298 (Rev. 8/98)
Prescribed by ANSI Std. Z39.18

AFOSR Final Report

Contract/Grant Title: Low-Density Hyper-Confined Molecular Hybrids: Multifunctional Design and Mechanical Behavior

Contract/Grant #: FA9550-16-1-0354

Reporting Period: 10/01/2018 - 09/30/2019

Author: Prof. Reinhold H. Dauskardt

Abstract

Our project focuses on low-density hybrid nanocomposites where polymers are confined at molecular length scales in a nanoporous matrix. Our goal is to develop a fundamental understanding of the effects of hyper-confinement in low-density hybrids, which provides guidelines for exploring the limits of strengthening and toughening to create mechanically robust hybrids for aerospace applications. We also exploit the opportunity of creating high-temperature low-density hybrids for aerospace applications by the combination of high-temperature low-density hybrid nanoporous matrix together with polyimides with superior temperature capabilities.

Main Accomplishments/Successes

A. Highlights include our Nature Materials 2016 paper where we showed that incorporation of high-molecular-weight polymers into a nanoporous hybrid matrix leads to an outstanding five-fold improvement in fracture properties while maintaining very low density. The work demonstrated a novel "molecular bridging" mechanism.

B. In our Nano Letters 2017 paper we fabricated high-temperature polyimide nanocomposites by filling the porous matrix with an AFRL developed heat-resistant poly(amic ester) precursor of Phenyl-Ethynyl-Terminated-Imide (AFRL-PETI) resin. The pore size was 7 nm and the precursor molecules were ~ 5 – 8 nm in length with a stiff backbone and low solubility suggesting potential challenges for filling the matric. However, once again extremely efficient filling was demonstrated and even more remarkably, subsequent imidization and crosslinking was achieved under such molecular confinement. The crosslinked polyimide was shown to toughen the nanocomposite by >80%.

C. We provided proof-of-concept that the pore surface chemistry of the porous matrix has a great impact on the chemical interaction between the molecularly confined polymer and the pore surface presented at the ACS 253rd National Meeting & Exposition 2017. We showed that polymer confinement increases the glass transition temperature, T_g, and stronger polymer-surface interaction leads to higher T_g. These results have implications for the thermomechanical stability and ageing behavior of the hybrids and also significantly affects the fracture toughness of the nanocomposite.

D. In our ACS Applied Materials and Interfaces 2018 paper we demonstrated the really intriguing result that oligomers in molecular-scale confinement can markedly toughen materials far beyond

rule-of-mixtures estimates even when inter-molecular entanglements are completely absent. The presence of these oligomers was also shown to improve the resistance of the nanocomposite to moisture-assisted cracking. The connected nanopore diameter in this work was either 1.2 nm or 3.5 nm, and the oligomer RMS end-to-end size ranged from 1.8 – 2.2 nm.

E. Polymer confinement has been realized in hybrid nanocomposites where individual polymer molecules are confined by a nanoporous matrix to dimensions less than the molecular size of the polymer as shown in our Advanced Functional Materials 2019 paper. Here we show that by functionalizing the interior pore surfaces of a nanoporous organosilicate matrix we can fill the pores with polystyrene molecules to achieve extreme levels of molecular confinement not previously possible. This provides opportunities for unique thermal and mechanical properties.

Research Contributions:

The research contributions include

1. Our AFOSR program has been very productive with 5 recent publications.

2. Our work has demonstrated a novel "molecular bridging" mechanism in which individual confined polymer chains are stretched and pulled out of the matrix behind an advancing crack tip, a toughening mechanism not found in other composite materials.

3. Demonstrating that nanocomposite high-temperature resistant materials can be fabricated by filling a porous matrix with AFRL developed heat-resistant poly(amic ester) precursor has provided a new platform and opportunities for nanocomposite hybrids with unprecedented combinations of toughness and thermal properties.

Transitions: (required for final report)

1. Methods to industry

Our research involving filling of nanoporous materials with a polymer filler has been used by industry to create interlayer dielectrics in semiconductor devices that are more resistant to damage during device processing. Filled nanocomposite materials are also being actively considered by several companies for improved thermal resistant coatings for high-temperature polymer components.

2. Students to employment (trained under grant)

Yusuke Matsuda, Ph.D. now at Dow Chemical Corporation, Boston, MA.
Scott G. Isaacson, Ph.D. now at Sensel Corporation, Santa Clara, CA.
Jade I. Fostvedt, M.S. now a Ph.D. student at UC Berkeley.
Can Wang, Ph.D. now at Apple Corporation, Santa Clara, CA.

3. Techniques to AFRL (correspondence with AFRL researchers)

As noted below, our work involves a very active and productive collaboration with Dr. Jeffery Baur, Dr. Hilmar Koerner, Dr. Timothy Pruyn and Dr. Vikas Varshney at USAF AFMC AFRL/RXCCP Wright-Patterson AFB.

Collaborations:

1. AFRL – active and productive collaboration with Dr. Jeffery Baur, Dr. Hilmar Koerner, Dr. Timothy Pruyn, Dr. Vikas Varshney, Dr. T. Gibson, Dr. G. Tandon and Dr. Davide Simone at USAF AFMC AFRL/RXCCP Wright-Patterson AFB.

2. DOD – none.

3. Others - we interact with AFOSR investigator Prof. Priestly at Princeton University on flash-DSC and related thermal properties of the hybrids.

4. Industry - Drs. Geraud Dubois, Kristelle Lionti and Robert Miller in the polymers group at the IBM Almaden Research Center.

5. Student Internships – each year we involve two UG summer students in our research who are supported by a UG research experience program through the Vice Provost for Undergraduate Education at Stanford.

Awards:

External recognition – five invited talks in 2019 presenting on our AFOSR research.

Publications:

1. Patents

None.

2. Journal

1. Can Wang, Scott G. Isaacson, Yucheng Wang, Krystelle Lionti, Willi Volksen, Teddie P. Magbitang, Mithun Chowdhury, Rodney D. Priestley, Geraud Dubois and Reinhold H. Dauskardt, "Surface Chemical Functionalization to Achieve Extreme Levels of Molecular Confinement in Hybrid Nanocomposites," **Advanced Functional Materials**, 1903132, 2019. DOI: 10.1002/adfm.201903132

2. Scott G. Isaacson, Yusuke Matsuda, Krystelle Lionti, Theo Frot, Willi Volksen, Reinhold H. Dauskardt, Geraud Dubois, "Using Unentangled Oligomers to Toughen Materials", **ACS Applied Materials and Interfaces**, DOI: 10.1021/acsami.8b03050, 2018.

3. Qiran Xiao, Joseph A. Burg, Yao Zhou, Hao Yan, Can Wang, Yichuan Ding, Evan Reed, Robert D. Miller, Reinhold H. Dauskardt, "Electrically Conductive Copper Core-Shell Nanowires through Benzenethiol-Directed Assembly", **Nano Letters**, 18 (8), pp. 4900-4907, 2018.

4. Farhan Ansari, Yichuan Ding, Lars A. Berglund, Reinhold H. Dauskardt, "Towards Sustainable Multifunctional Coatings Containing Nanocellulose in a Hybrid Glass Matrix," **ACS Nano**, DOI: 10.1021/acsnano.8b01057, 2018.

5. Scott G. Isaacson, Jade I. Fostvedt, Hilmar Koerner, Jeffery W. Baur, Krystelle Lionti, Willi Volksen, Geraud Dubois, Reinhold H. Dauskardt, "Synthesis of Polyimides in Molecular-Scale Confinement for Low-Density Hybrid Nanocomposites", **Nano Letters**, 17 (11), pp. 7040-7044, 2017.

6. Scott G. Isaacson, Krystelle Lionti, Willi Volksen, Teddie P. Magbitang, Yusuke Matsuda, Reinhold H. Dauskardt, Geraud Dubois, "Fundamental Limits of Material Toughening with Molecularly Confined Polymers", **Nature Materials**, 15 (3), pp. 294-298, 2016.

Software:

None.

Invited Talks (recent only):

1. DOD meetings

2. Professional Societies

November 2019, "Exploiting Extreme Molecular-Confinement in Dielectric Hybrids for Enhanced Mechanical and Thermal Behavior," invited presentation at the 16th International Conference on. Reliability and Stress-related Phenomena in Nano and Microelectronics, San Jose, CA.

August 2019, "Molecular Engineering at the Extreme Limits of Molecular-Scale Confinement," invited presentation at the 2019 Fall Meeting of the American Chemical Society, Orlando, FL.

April 2019, "Molecular Design and Engineering of Low-Density Hybrids at the Extreme Limits of Molecular-Scale Confinement," invited presentation at the 2019 Spring Meeting of the American Chemical Society, Orlando, FL.

April 2019, "Nanomaterials Design and Properties at the Extreme Limits of Molecular-Scale Confinement," invited presentation at the Spring MRS conference, Phoenix, AZ.

3. Students

4. AFOSR PI Meeting

The 2019 Low Density Materials Review held July 8-10, 2019 at the WBI Springfield Street (Wright Brothers Institute Springfield Street). Presentation entitled: "Molecular Design and Engineering of Low-Density Hybrids at the Extreme Limits of Molecular-Scale Confinement" by Reinhold Dauskardt.

Community Efforts:

1. Data Collects

2. Student events

References:

Publications resulting from the grant are noted above.

Changes in Research Objectives: None
Change in AFOSR Program Manager: Dr. Jamie Tiley replaced Dr. Joycelyn Harrison
Extensions Granted or Milestones Slipped: None.
New discoveries, inventions, or patent disclosures: Noted above.

Append 1 – 3 Published Papers to the PDF file before submitting

FULL PAPER

Polymer Confinement

ADVANCED
FUNCTIONAL
MATERIALS

www.afm-journal.de

Surface Chemical Functionalization to Achieve Extreme Levels of Molecular Confinement in Hybrid Nanocomposites

Can Wang, Scott G. Isaacson, Yucheng Wang, Krystelle Lionti, Willi Volksen, Teddie P. Magbitang, Mithun Chowdhury, Rodney D. Priestley, Geraud Dubois,* and Reinhold H. Dauskardt*

Polymer confinement is realized in hybrid nanocomposites where individual polymer molecules are confined by a nanoporous matrix to dimensions less than the molecular size of the polymer. Here it is shown that by functionalizing the interior pore surfaces of a nanoporous organosilicate matrix, the pores can be filled with polystyrene molecules to achieve extreme levels of molecular confinement not previously possible. This provides opportunities for unique thermal and mechanical properties. It is shown that pore surface functionalization markedly impacts the polymer mobility during polymer infiltration by affecting the polymer–pore surface interaction, addressing the challenge of filling high-molecular-weight polymer molecules into nanoscale-confined spaces. This allows for achieving extreme levels of molecular confinement with the loss of interchain entanglement and extensive polymer elongation along the pore axis. The glass transition temperature of the polymer is suppressed compared to bulk polymer melt, and is significantly affected by the polymer–surface interaction, which changes the polymer segmental mobility. The polymer–surface interaction also affects the interfacial polymer–pore sliding shear stress during polymer pullout from the nanopores, markedly affecting the fracture resistance of the nanocomposite.

1. Introduction

Polymer confinement in nanocomposites influences properties including the glass transition temperature (T_g) of the polymer[1] as well as the stiffness[2] and viscoelastic behavior[3] of the nanocomposites. Molecular polymer confinement can be achieved by filling polymer molecules into a nanoporous matrix with a pore size less than the bulk root-mean-square end-to-end distance

of the polymer, which has been shown to reduce entanglements,[4] form ordered morphology,[5] influence T_g,[6] improve polymer diffusivity,[7] and enhance fracture resistance of the nanocomposites.[8] A fundamental limit of these studies, however, has been to achieve extreme levels of molecular confinement and the ability to control the interfacial interaction of the confined polymer with the matrix pores.

Here we demonstrate that pore surface chemical functionalization allows us to achieve extreme levels of molecular confinement and manipulate the nanocomposite thermal and mechanical properties by controlling the interaction of the polymer with the pore surface (**Figure 1**). We show that the polymer filling rate can be significantly improved through selection of appropriate surface chemistry, which enables filling polymers with unprecedentedly high molecular weight (M_w) into the porous matrix to create extreme levels of molecular confinement not previously possible. This induces polymer hyperconfinement[[8a]] in which polymer chains entirely lose interchain entanglements and elongate extensively along the pore axis.[9] We also show that T_g of the polymer is decreased by hyperconfinement, and can be significantly affected by tuning the polymer–surface interaction to impact the polymer segmental mobility.

In addition, we show that the polymer–surface interaction affects the fracture of the nanocomposites where molecular

C. Wang, Dr. S. G. Isaacson, Dr. G. Dubois, Prof. R. H. Dauskardt
Department of Materials Science and Engineering
Stanford University
496 Lomita Mall, Stanford, CA 94305, USA
E-mail: gdubois@us.ibm.com; dauskardt@stanford.edu
Y. Wang, Prof. R. D. Priestley
Department of Chemical and Biological Engineering
Princeton University
Engineering Quadrangle, Princeton, NJ 08544, USA

Dr. K. Lionti, Dr. W. Volksen, T. P. Magbitang
Hybrid Polymeric Materials
IBM Almaden Research Center
650 Harry Road, San Jose, CA 95120-6099, USA
Dr. M. Chowdhury
Metallurgical Engineering and Materials Science
Indian Institute of Technology Bombay
Mumbai 400076, India
Dr. G. Dubois
Science to Solutions
IBM Almaden Research Center
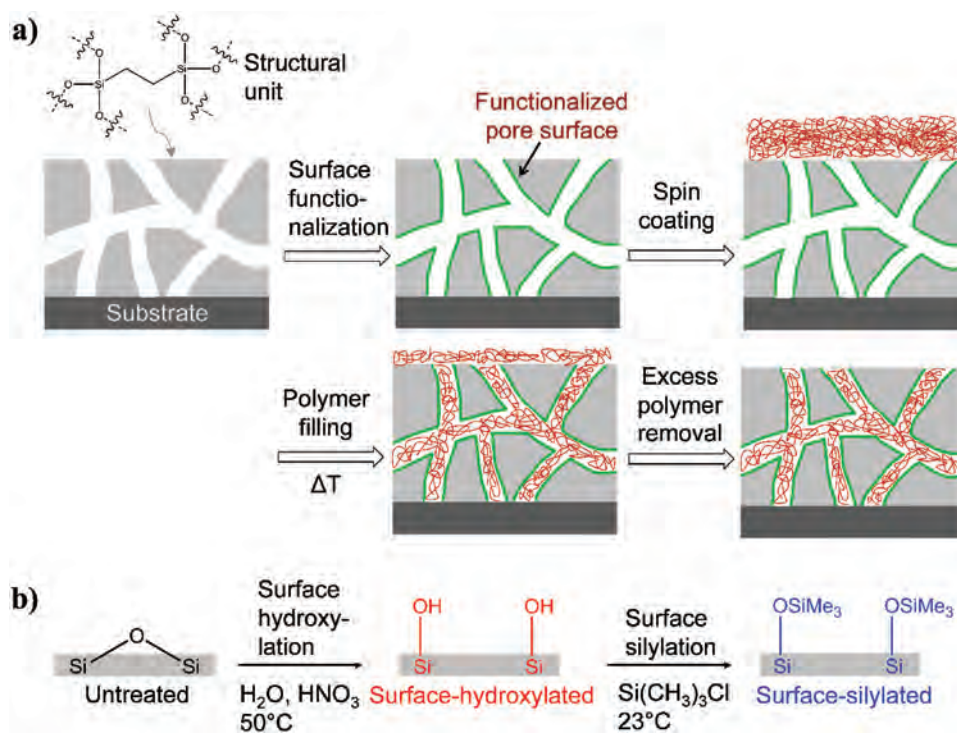650 Harry Road, San Jose, CA 95120-6099, USA

Figure 1. a) Schematics of the structural unit of the matrix as well as the fabrication steps of the hybrid nanocomposites showing the sequence of functionalizing the pore surfaces, spin-coating of polymer (which is polystyrene in this work) on top of the matrix, polymer filling at elevated temperature, and removal of excess polymer by solvent wash. b) Major surface chemical reactions during surface functionalization.

bridging that involves the pullout and stretching of individual confined polymer chains from the nanopores leads to a marked increase in fracture resistance. The surface chemical functionalization significantly changes the sliding shear stress at the polymer/pore surface interface during the pullout, allowing manipulation of the fracture resistance.

2. Results and Discussion

Three types of pore surfaces with different surface chemistry were employed in this study (Figure 1), namely hydroxylated, untreated, and silylated pore surfaces (listed in the order of increasing hydrophobicity). The starting material was the untreated matrix, an ethylene-bridged organosilicate (Et-OCS) thin film with a porosity of 42.0% and a thickness of ≈600 nm.[10] The percolating pore network in the untreated matrix consisted of approximately cylindrical pores of which the average pore diameter was 7.8 nm (Figure S5, Supporting Information). The major chemical groups on the pore surface of the untreated matrix were siloxane groups (Si−O−Si), Si−CH$_2$−CH$_2$−Si bridges, and some silanol groups (Si−OH). To alter the surface chemistry, we first used nitric acid to catalyze the surface hydroxylation reaction in which surface siloxane groups reacted with water to form surface silanol groups (Si−O−Si + H$_2$O → 2SiOH), making the surface hydrophilic. We then silylated the surface by taking advantage of the reaction between trimethylchlorosilane and surface silanol groups (Si−OH + Cl−Si(CH$_3$)$_3$ → Si−O−Si(CH$_3$)$_3$ + HCl), making the surface hydrophobic. Fourier transform infrared

spectroscopy (FTIR), water contact angle measurement, and ellipsometric porosimetry (EP) were used to characterize the functionalized surface.

FTIR spectra showed that after the surface hydroxylation, a sharp peak corresponding to free (isolated and germinal) silanol groups at 3732 cm^{-1} and a broad peak at 3400–3600 cm^{-1} corresponding to hydrogen-bonded silanol groups[11] increased significantly, indicating that the surface hydroxylation to form silanol groups was successful (**Figure 2**a). After the surface silylation, the hydrogen-bonded silanol peak decreased and the free silanol peak was completely eliminated, which was consistent with a previous study.[12] The appearance of the peak corresponding to C−H in −CH$_3$ at 2962 cm^{-1} after the surface silylation further proved that trimethylsilyl groups were grafted on the surface.[13]

Water contact angles measurements on the top surface of the three types of matrices provided additional evidence showing that both the surface hydroxylation and silylation were successful. Water contact angles of the untreated, surface-hydroxylated, and surface-silylated matrices were measured to be 62°, <15°, and 87°, respectively. These results showed that surface hydroxylation made the matrix surface hydrophilic, while surface silylation of the hydroxylated surface not only eliminated such hydrophilicity, but also made the surface more hydrophobic than the original, untreated surface. These observations are expected for successful surface hydroxylation and silylation reactions.

In order to gain insight into the chemical interaction of the polymer filler (which is polystyrene (PS) in this work) with the nanopore surface, we used EP with toluene, an analog of
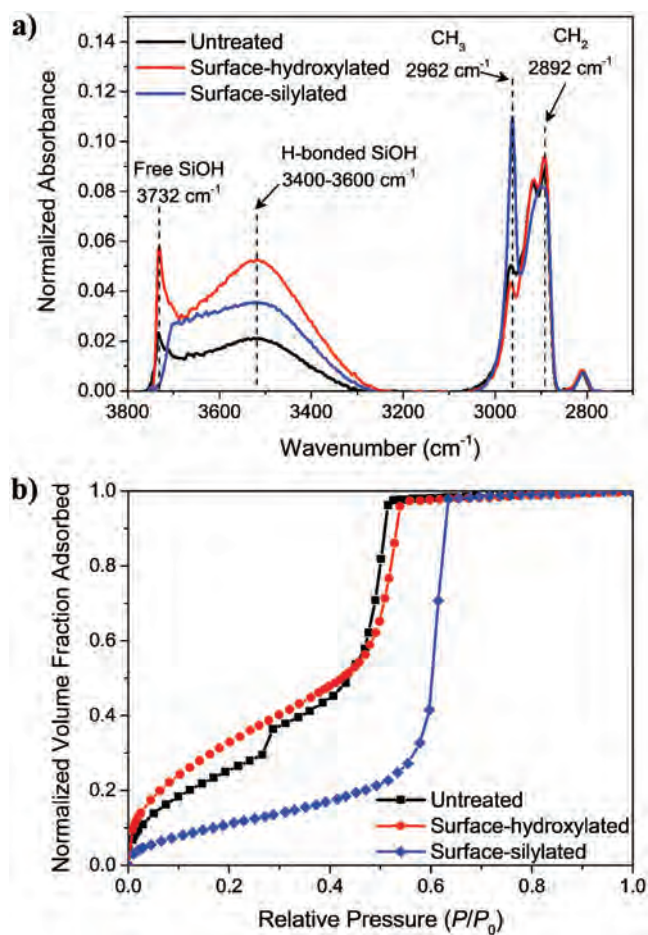
**ADVANCED
SCIENCE NEWS**
www.advancedsciencenews.com

**ADVANCED
FUNCTIONAL
MATERIALS**
www.afm-journal.de

Figure 2. Characterization results of the untreated, surface-hydroxylated, and surface-silylated matrices, including a) FTIR spectra and b) adsorption branches of EP using toluene as the adsorbate.

PS, as the adsorbate. EP measurements of the three types of nanoporous matrices showed that the adsorption isotherms for the untreated and surface-hydroxylated matrices were similar, while the adsorption curve for the surface-silylated matrix was very different from the others (Figure 2b). At low relative pressures where monolayer adsorption dominated and was sensitive to surface chemistry, toluene adsorption was improved by the surface hydroxylation and dramatically suppressed by the surface silylation. Even at medium relative pressures where multilayer adsorption took place and was less sensitive to surface chemistry, the surface silylation still led to a much smaller slope in the adsorption curve whereas the other two types of matrices displayed similar slopes. Combined with the fact that the surface silylation also pushed the pressure of capillary condensation from P/P_0 of ≈0.5 to ≈0.6, this phenomenon indicated that the chemical interaction between toluene molecules and the silylated surface was so weak that even multilayer adsorption was strongly hindered, which delayed the capillary condensation.

Suppression of adsorption and delay of capillary condensation have also been observed in water adsorption on hydrophobic mesoporous silica compared to the same material but after surface hydroxylation,[14] which is intuitive since the interaction of water with the hydrophobic surface is weak. However in the present study, the fact that the interaction of toluene (a hydrophobic molecule) with the surface decreases with increasing surface hydrophobicity may seem counterintuitive, as it seems to violate the "like dissolves like" rule. This result can be understood by similar benzene adsorption studies on silica surfaces. Benzene adsorption on silica is strongly affected by the concentration of surface silanol groups[11,15] due to the hydrogen bonding between surface silanol groups and the π electrons of benzene.[16] The heat of adsorption of benzene on silica with different surface chemistries has been shown to follow the order of surface-hydroxylated silica > surface-dehydroxylated silica > surface-silylated silica,[17] since surface dehydroxylation and surface silylation decrease the density of surface silanol groups. The presence of trimethylsilyl groups on the silylated silica surface also blocks benzene from the surface, which contributes to a drop in the adsorption potential and leads to even greater adsorption reduction.[15,17]

The aforementioned EP results suggest that the surface hydroxylation increases the PS–surface chemical interaction through addition of surface silanol groups, while the surface silylation decreases this interaction by eliminating surface silanol groups and adding surface trimethylsilyl groups. This is supported by further characterizations including the FTIR data of the PS-filled surface-hydroxylated matrix showing a shift of the silanol peak after PS filling, dewetting of low-M_w PS on the surface of the surface-silylated matrix, and the phenomenon of low-M_w PS being washed out of the pores of the filled surface-silylated matrix by toluene (Discussion S1, Supporting Information).

We then demonstrate how the surface functionalization of the porous matrix impacts polymer mobility when filling the polymer into the matrix, and how that facilitates the achievement of polymer hyperconfinement in hybrid nanocomposites. We fabricated hybrid nanocomposite thin films by three steps (Figure 1): 1) PS was spin-coated on top of the matrix; 2) the sample was heated in an inert atmosphere to allow polymer infiltration into the nanopores; 3) the excess PS on top of the matrix was removed by a toluene rinse while the confined PS remained in the pores because they got "stuck." We note that, as mentioned in the previous paragraph, when PS with $M_w \leq 101$ kDa was used to fill the surface-silylated matrix, the confined PS was removed by the toluene rinse due to the weak PS–surface interaction (Discussion S1, Supporting Information). We found that PS over a wide range of M_w from 50 to 3260 kDa can be used to completely fill the matrix, as confirmed by X-ray reflectivity (XRR) and depth-profiling X-ray photoelectron spectroscopy (DP-XPS) (**Figure 3**, **Table 1**; Table S1a–c, Supporting Information). We observed that the pore surface chemistry had a large impact on the rate of polymer infiltration into the pores. When PS M_w is ≤ 426 kDa, all the three types of matrices can be completely filled using a 300 °C/1 h filling condition. When PS M_w is 1.29 MDa, using the same 300 °C/1 h filling condition resulted in incomplete filling of the untreated and surface-hydroxylated matrix due to decreased PS melt mobility at higher M_w, but it resulted in complete filling of the surface-silylated matrix. We observed that the PS molecules only infiltrated through the top 59% and 69% of the total thickness for
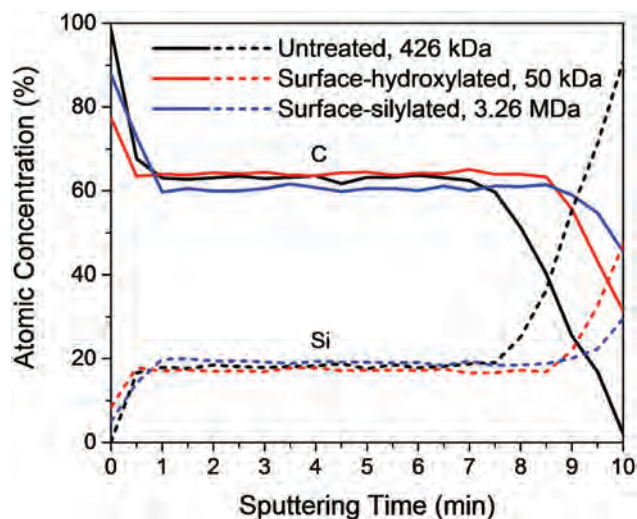
DISTRIBUTION A: Distribution approved for public release.

**ADVANCED
SCIENCE NEWS**
www.advancedsciencenews.com

**ADVANCED
FUNCTIONAL
MATERIALS**
www.afm-journal.de

Figure 3. DP-XPS results of three representative hybrid nanocomposites show flat plateaus in the carbon and silicon concentrations of all the nanocomposites, providing evidence for uniform dispersion of PS through the whole film thickness. The plateau carbon and silicon concentrations of the unfilled matrix are ≈23–29% and ≈35–37%, respectively (depending on the matrix type). Knowing the chemical compositions of the unfilled matrix and PS, we estimate that a completely filled untreated, surface-hydroxylated, and surface-silylated nanocomposites would exhibit a plateau carbon concentration of ≈62%, ≈58%, and ≈56%, respectively. All the nanocomposites are completely filled since all the measured plateau carbon concentrations are slightly higher than the corresponding estimates.

the untreated and the surface-hydroxylated matrix, respectively (Table S1d, Supporting Information). In fact, the 300 °C/1 h filling condition even allowed complete filling of the surface-silylated matrix with 3.26 MDa PS.

A fluid flow model can be employed to explain how the surface chemistry affects the polymer chain mobility and the polymer filling rate. The imbibition of a polymer melt into nanopores is driven by capillary forces. Treating the polymer melt as a fluid, the penetration depth (x) of the polymer melt into a capillary can be described by the classical Lucas–Washburn (L–W) model[18]

$$x = \sqrt{\frac{r_{pore}\gamma\cos\theta}{2\eta}} \cdot \sqrt{t} \qquad (1)$$

where r_{pore} is the pore radius, γ is the surface tension of the liquid, θ is the contact angle between the pore surface and the meniscus, η is the viscosity of the fluid, and t is the time.

Higher η represents lower polymer mobility. The L–W model has been verified experimentally for the infiltration of molecularly confined polymer melts into nanopores.[7,19] In classical fluid dynamics, η represents the internal friction between fluid molecules, but in the case of molecularly confined polymer, η should be regarded as the effective viscosity mainly representing the polymer–surface friction rather than the polymer–polymer internal friction for two reasons: 1) the interchain entanglement decreases with increasing extent of confinement (EC) and eventually disappears at a critical extent of confinement (see the detailed discussion in the following paragraph); 2) the extremely high interfacial surface-to-volume ratio for molecularly confined polymer chains and therefore the polymer–surface friction must contribute substantially to the total friction. When we apply the L–W model to our case, we see that the surface silylation has two opposing effects on the filling rate. On the one hand, the surface silylation leads to a higher θ (due to weaker polymer–surface chemical interaction) and a smaller r_{pore} (Discussion S4, Supporting Information), both of which oppose a higher filling rate. On the other hand, the weaker polymer–surface chemical interaction should and has to decrease η in order to result in an increased filling rate. In fact, previous works on nonmolecularly confined polymers have revealed that a weaker polymer–surface interaction decreased η.[20] In the case of the surface silylation, the effect of lower η dominates and leads to a higher filling rate. The surface hydroxylation has exactly the opposite effects of the surface silylation (lower θ, higher r_{pore} and η), and turns out to give an equivalent or slightly faster filling rate.

Facilitating polymer filling through the surface silylation is a powerful strategy to achieve hyperconfinement of polymers. Scaling arguments have shown that polymer chains in a melt confined in a cylindrical pore do not elongate along the pore axis until the EC reaches a critical value at the onset of hyperconfinement.[9] The interchain entanglement density decreases with EC and vanishes at the onset of hyperconfinement. Once the onset of hyperconfinement begins, elongation of the polymer chains along the pore axis occurs with increasing EC, which can be obtained by increasing the M_w (leading to higher η) and/or decreasing the r_{pore}. The L–W model indicates that both approaches will decrease the filling rate. We also note that although polymer mobility can be enhanced by confinement before reaching hyperconfinement,[7] it will be suppressed when hyperconfinement is achieved,[21] therefore, will again lead to a slowdown in the filling rate. Thus, the surface silylation is crucial for obtaining higher EC while maintaining a reasonably rapid filling rate. We leveraged the surface-silylated matrix to achieve a complete fill with PS of a very high M_w (3.26 MDa) using a 300 °C/1 h filling condition (Figure 3 and Table 1).

To quantify the EC that the 3.26 MDa PS chain experienced and determine whether hyperconfinement was achieved, we first define EC as $\langle r^2 \rangle_0^{1/2}/d_{pore}$, where $\langle r^2 \rangle_0^{1/2}$ is the square root of the mean-squared end-to-end distance of the bulk polymer and d_{pore} is the pore diameter. The critical EC at the onset of hyperconfinement is d_{pore}/a, where a is the

Table 1. XRR results of the three representative nanocomposites also confirm complete filling. The method for fill level calculation is described previously.[31] A complete list of XRR results of all the nanocomposites we have investigated is in Table S1 (Supporting Information).

Nanocomposite type	Density of unfilled matrix [g cm⁻³]	Density after filling [g cm⁻³]	Fill [%]
Untreated, 426 kDa PS	0.799	1.274	100
Surface-hydroxylated, 50 kDa PS	0.860	1.312	100
Surface-silylated, 3.26 MDa PS	0.897	1.315	100

Kuhn length of the polymer.[9] The number of Kuhn monomers (N) at the critical EC is defined as N_c

$$N_c = \left(\frac{d_{pore}}{a}\right)^4 \tag{2}$$

In the case of polystyrene ($a = 1.8$ nm) confined in the surface-silylated matrix ($d_{pore} = 7.2$ nm; Discussion S4, Supporting Information), $N_c = 256$, corresponding to an M_w of 184 kDa. For the untreated and surface-hydroxylated matrices, hyperconfinement of PS starts at M_w of ≈253 kDa due to slightly larger pore size. For a confined polymer possessing N Kuhn monomers, the completion degree of hyperconfinement (θ) can be defined to describe how close the current confinement state is to the onset of hyperconfinement

$$\theta = \frac{N}{N_c} \times 100\% \tag{3}$$

Experimental results from literatures are in good agreement with the scaling arguments described earlier. Polymers confined in a nanoporous membrane were shown to preserve their bulk radius of gyration along the pore axis at least up to an EC of ≈4.9 and a θ of ≈35%, and the ratio of the effective viscosity of the confined polymer-to-bulk viscosity (RV) was shown to decrease with θ due to reduced interchain entanglement.[7] At $\theta \cong 83\%$, RV was found to be ≈10^4, corresponding to an increase in the number of Kuhn monomers between entanglements (N_e) by a factor of ≈700, which was consistent with the scaling argument that N_e should be infinity when $\theta \geq 100\%$. At a θ of ≈1%, a small increase of 32% in N_e was measured experimentally.[4b]

Here, having 3.26 MDa PS in the surface-silylated pores with $d_{pore} = 7.2$ nm corresponds to an EC of 16.8 and a θ of 1740%, meaning that the confinement of the polymer is far beyond the onset of hyperconfinement. To our knowledge, the highest EC and θ that have been reported by others were ≈7.6 and ≈83%, respectively.[7] We achieved EC = 10.6 and θ = 710% recently,[8a] and now we exceed this limit by exploiting the surface chemistry. Such large EC and θ values lead to extensive chain elongation along the pore axis. The extension ratio (ER) can be defined as the extended end-to-end distance along the pore axis ($\langle r^2 \rangle_{\parallel}^{1/2}$) over $\langle r^2 \rangle_0^{1/2}$.

$$ER = \frac{\langle r^2 \rangle_{\parallel}^{1/2}}{\langle r^2 \rangle_0^{1/2}} = \frac{Na^3 d_{pore}^{-2}}{aN^{1/2}} = \frac{a^2 N^{1/2}}{d_{pore}^2} \tag{4}$$

ER for 3.26 MDa PS confined in 7.2 nm pores is ≈420%, compared to our previous result with an ER of ≈271%.

The strong dependence of polymer mobility on surface chemistry suggests a strong dependence of T_g on surface chemistry. Here, we demonstrate the effect of polymer–surface interaction on T_g of hyperconfined polymers. T_g values of bulk and molecularly confined polymers were measured by flash differential scanning calorimetry (flash-DSC) at a heating rate of 8000 K s^{-1} (**Figure 4**). Molecular confinement of PS in the nanocomposite decreases T_g of the polymer for all the samples investigated, consistent with previous reports on molecularly confined (but not hyperconfined) polymers in cylindrical pores showing

decreased T_g,[6] and enhanced segmental mobility.[22] We note that the T_g values of bulk PS we measured on PS powder are higher than what have been reported using conventional DSC (105–107 °C)[23] because the heating rate employed in our flash-DSC measurement is six orders of magnitude higher than what is used in conventional DSC.

For hyperconfined PS ($M_w = 426$ kDa, $\theta \cong 170\%$, EC ≅ 5.6), the pore surface hydroxylation increases T_g above the untreated pore surfaces by ≈5.5 °C while the pore surface silylation decreases it below the untreated pore surfaces by ≈7.5 °C. For molecularly confined but not hyperconfined PS ($M_w = 50$ kDa, $\theta \cong 20\%$, EC ≅ 1.9), the pore surface hydroxylation also increases T_g above the untreated pore surfaces by ≈13 °C. This demonstrates that stronger PS–surface interaction decreases the segmental mobility of confined PS and leads to higher T_g. Previous report on nonmolecularly confined polymers agrees with our results, showing that stronger polymer–surface interaction increases T_g.[24]

Preliminary results obtained show that the pore surface chemistry affects how increasing confinement level (increasing M_w for the same pore size) changes ΔT_g (which is confined T_g minus bulk T_g, always negative). Increasing M_w from 50 to 426 kDa makes ΔT_g of surface-hydroxylated nanocomposite significantly more negative but essentially does not affect ΔT_g of untreated nanocomposite. Askar et al. have shown that molecular confinement (but not hyperconfinement) of PS in the cylindrical nanopores of anodic aluminum oxide (AAO) templates makes ΔT_g negative, and ΔT_g becomes more negative with increasing M_w for the same pore size,[6] which is consistent with the $\Delta T_g - M_w$ relationship in the case of surface-hydroxylated nanocomposite in our work. Such a consistency is likely due to the fact that the interaction between PS and AAO surface is comparable to the interaction between PS
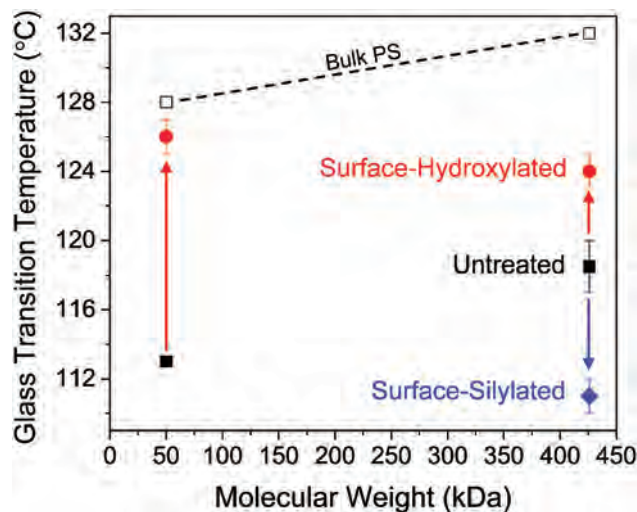

Figure 4. T_g values as a function of molecular weight of bulk PS (black open squares) and confined PS in the nanocomposites with different pore surface chemistry, measured by flash-DSC. The black filled squares, red filled circles, and blue filled diamonds correspond to PS confined in untreated, surface-hydroxylated, and surface-silylated nanocomposites, respectively. All T_g values are determined at half-devitrification at 8000 K s^{-1} heating. Note that surface-silylated nanocomposite with 50 kDa PS cannot be fabricated because excess PS removal by toluene wash would remove the confined PS from the surface-silylated pores.

**ADVANCED
SCIENCE NEWS**

www.advancedsciencenews.com

**ADVANCED
FUNCTIONAL
MATERIALS**

www.afm-journal.de

and the hydroxylated surface. Similar to the hydroxylated surface in this work, AAO surface is hydrophilic and has a lot of surface hydroxyl groups that can interact with PS (the water contact angle of nonporous AAO surface has been reported to be 13°).[25] The $\Delta T_g - M_w$ relationship in the work of Askar et al. only magnifies at high molecular weight ≈1 MDa, while we can achieve such a dependence at lower molecular weight by hyperconfinement. Future studies should concentrate on the $\Delta T_g - M_w$ relationship by investigating a much broader range of M_w and understanding the fundamental reason for the $\Delta T_g - M_w$ trend.

We finally show how the surface functionalization impacts fracture of the nanocomposites by changing the polymer–surface interfacial sliding shear stress during pullout and the fracture resistance. During the fracture of the nanocomposites, the crack surfaces near the crack tip are bridged by individual polymer molecules, which is a molecular-scale analog of fiber bridging in conventional fiber-reinforced composites. Crack growth is resisted by the pullout of the polymer molecules from the pores, leading to an increased cohesive fracture energy (G_c).[8a] Double cantilever beam (DCB) fracture tests were used to measure G_c of the nanocomposites. All the fracture samples were completely filled with polymer under a 300 °C/1 h filling condition, except for only one sample which was the untreated nanocomposite with 1.29 MDa PS, the filling time had to be increased 3 h to achieve complete filling. We note that some fracture samples are impossible to be fabricated, which are the surface-hydroxylated nanocomposite with 1.29 MDa PS and the surface-silylated nanocomposites with ≤101 kDa PS (Discussion S2, Supporting Information). All three types of nanocomposites displayed the same qualitative fracture behavior, which was that G_c increased with the PS M_w before reaching a
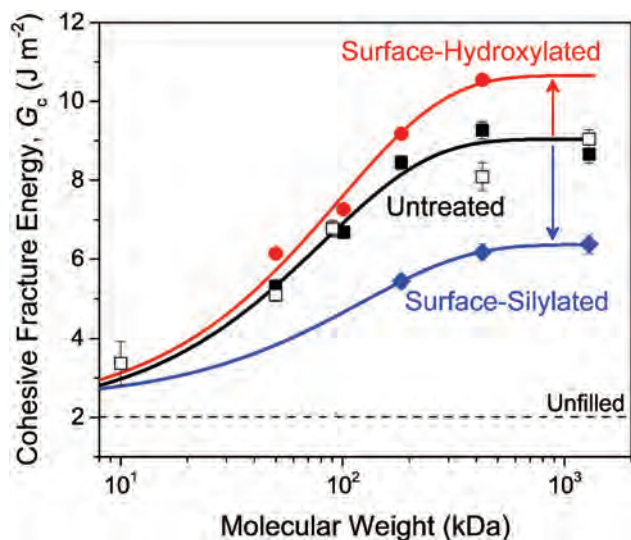

Figure 5. Cohesive fracture energy, G_c, of the untreated (black filled squares), surface-hydroxylated (red filled circles), and surface-silylated (blue filled diamonds) nanocomposites with PS filler over a wide range of PS M_w. The solid red, black, and blue curves are fits of the molecular strength–limited bridging model for the untreated, surface-hydroxylated, and surface-silylated nanocomposites, respectively. The black open squares are the previous results of untreated nanocomposites.[8a] G_c of an unfilled matrix is ≈2 J m⁻².

plateau at ≈400 kDa (**Figure 5**). This overall trend of G_c with respect to M_w has been explained previously that the energy dissipated during the molecular bridging increases with the pullout length of the confined polymer, and the pullout length initially increases with M_w but is ultimately limited due to chain breakage by high pullout stress at high M_w.[8a] We note that hyperconfinement of PS does not show an effect on G_c. For the investigated range of M_w, G_c of the nanocomposite was increased by the surface hydroxylation and decreased by the surface silylation. Therefore, G_c of the nanocomposite rises with the polymer–surface chemical interaction strength. The effect of the surface functionalization was dramatic, as the G_c of the surface-hydroxylated nanocomposite was ≈70% higher than that of the surface-silylated nanocomposite at the plateau value of G_c. Note that the untreated nanocomposite exhibited G_c values that were consistent with the values of a previous batch we studied.[8a] In that previous batch, the untreated nanocomposite with 1.29 MDa PS was completely filled using a 300 °C/1 h condition, and the G_c of that sample was consistent with the G_c of the present sample fabricated using a 300 °C/3 h filling condition. So the filling time for the 1.29 MDa PS did not affect G_c.

Fitting the data for G_c as a function of M_w with a molecular strength–limited bridging model enables us to quantify the impact of the surface functionalization on the sliding shear stress (τ) at the interface between the polymer and the pore surface during the pullout. We showed previously that G_c of the hybrid nanocomposite is[8a]

$$G_c = G_0 + \frac{1}{2} f\beta\delta_0^2 (1 + \varepsilon_{\max}) \tag{5}$$

where G_0 is the cohesive fracture energy of the unfilled matrix, f is the polymer volume fraction in the nanocomposite, $\varepsilon_{\max}$ is the theoretical maximum strain for a single entangled chain, δ_0 is the maximum pullout length, and β is the proportionality constant between the maximum bridging stress (σ_0) and δ_0

$$\beta = \frac{\sigma_0}{\delta_0} \tag{6}$$

Here, we show that β is directly related to τ. The bridging force is equal to the shear force due to a simple force balance. By treating the confined polymers as cylindrical "fibers," we have

$$\tau \cdot \pi d_{\text{pore}} \, \delta_0 = \sigma_0 \cdot \frac{\pi}{4} d_{\text{pore}}^2 \tag{7}$$

Rearrangement of this equation gives

$$\frac{\sigma_0}{\delta_0} = \frac{4\tau}{d_{\text{pore}}} = \beta \tag{8}$$

Now, G_c of the hybrid nanocomposite can be rewritten as

$$G_c = G_0 + \frac{2f\tau}{d_{\text{pore}}} \delta_0^2 (1 + \varepsilon_{\max}) \tag{9}$$

As mentioned previously, G_c scales with $\tau\delta_0^2$.

If no chain breakage happens, δ_0 is assumed to be half the end-to-end distance of a single polymer chain, $\delta_0 = \frac{1}{2}\langle r^2 \rangle_0^{1/2} = \frac{1}{2} a N^{1/2}$. However, high forces are generated at high molecular weight and rupture polymer backbone bonds, which limit δ_0 and thus G_c. In an extension of the bridging model, here we assume that δ_0 of the broken chains follows a half-normal distribution (δ_0 is non-negative) and show that (Discussion S3, Supporting Information)

$$G_c = G_0 + \frac{2f\tau}{d_{\mathrm{pore}}} \left[\frac{1}{4} a^2 \mathrm{Nerfc}\left(\frac{a\sqrt{N}}{2\sqrt{2}c} \right) - \frac{ca\sqrt{N}}{\sqrt{2\pi}} e^{-\frac{a^2 N}{8c^2}} + c^2 \mathrm{erf}\left(\frac{a\sqrt{N}}{2\sqrt{2}c} \right) \right] (1 + \varepsilon_{\max})$$

(10)

where c is the scale parameter of the half-normal distribution. Values of d_{pore}, f, and G_0 are obtained from experiments (Discussions S4 and S5, Supporting Information), and $\varepsilon_{\max}$ is ≈ 3 for PS.[26] Therefore, τ and c are the only two fitting parameters.

This molecular strength–limited bridging model captures the fracture behavior of all three types of nanocomposites over a broad range of polymer molecular weight, and provides information of the polymer–surface chemical interaction strength by the value of τ (Figure 5). Fitting this model to the fracture energy data yields τ values of 239, 257, and 102 MPa for the untreated, surface-hydroxylated, and surface-silylated nanocomposites, respectively. τ is increased by the surface hydroxylation and decreased by the surface silylation, which is expected since higher polymer–surface interaction should increase the sliding friction at the interface, and therefore should increase τ. In conventional fiber-reinforced composites, surface chemical functionalization has also been shown to effectively change the fiber–matrix chemical interaction and, as a result, the fracture energy, interfacial debonding shear stress, and interfacial sliding shear stress.[27] Our result further illustrates how dramatically the surface functionalization can change the polymer–surface chemical interaction, as the τ of the surface-hydroxylated nanocomposite is $\approx 152\%$ higher than the surface-silylated nanocomposite. This difference in the τ is much higher than the G_c difference of these two nanocomposites. Previous studies have shown that the friction coefficient of bulk PS on a hydrophilic, hydroxyl-terminated silicon wafer was $\approx 190\%$ higher than the friction coefficient of PS on a hydrophobic, methyl-terminated silicon wafer,[28] which is in good agreement with our result of $\approx 152\%$.

The value of τ observed in conventional polymer–fiber composites is usually around 1–55 MPa,[27c,29] which is smaller than what we obtain in this work. As the bridging force is high enough to rupture backbone bonds of PS molecules in our hybrid nanocomposites, the shear force and the shear stress should be correspondingly high (since the shear force is equal to the bridging force due to force balance). We can estimate the magnitude of τ without introducing a complex model. By definition, at the beginning of the pullout, τ is given by

$$\tau = \frac{F_{\mathrm{Shear,\,max}}}{\pi d_{\mathrm{pore}} \delta_0}$$

(11)

where $F_{\mathrm{Shear,\,max}}$ is the maximum shear force (which is equal to the maximum bridging force). When $M_w \cong 400$ kDa, the G_c of the nanocomposite reaches a plateau, meaning that the maximum bridging force reaches the ultimate tensile strength of the molecule (≈ 38 nN)[8a,30] and significant chain rupture occurs. At such M_w, we assume that chain rupture would decrease δ_0 to 50% of the value if there were no chain rupture, which gives $\delta_0 = 10$ nm. Using $F_{\mathrm{Shear,\,max}} = 38$ nN, $\delta_0 = 10$ nm, and $d_{\mathrm{pore}} = 7.8$ nm in the equation above yields an estimated τ of 160 MPa, which is of the same order of magnitude as the τ values obtained by using the strength-limited molecular bridging model.

3. Conclusion

This work demonstrates that surface chemical functionalization is a successful strategy to achieve unprecedented level of polymer hyperconfinement and manipulate the thermal and fracture properties of the hybrid nanocomposites. It also gives insights into how the polymer–surface chemical interaction impacts the mobility of molecularly confined polymer and the fracture of hybrid nanocomposites. Our findings provide a candidate material system for fundamental research of polymer hyperconfinement, and can be used to guide the design of multifunctional nanoscale devices containing molecularly confined polymers to achieve desired thermal and mechanical properties.

4. Experimental Section

Chemicals: Nitric acid (1 M), trimethylchlorosilane (TMCS), *n*-hexane, and PS (analytical standard with low dispersity) were purchased from Sigma-Aldrich. Acetone was purchased from Fisher Scientific.

Surface Functionalization of the Nanoporous Matrix: The Et-OCS matrix was obtained by spin-casting and thermally curing a porogen-containing sol–gel formulation on top of a 200 mm silicon wafer coated with a dense Et-OCS adhesion layer.[8a,10] The silicon wafer substrate was then diced into 50 × 50 mm square coupons. To hydroxylate the pore surfaces of the nanoporous matrix, an untreated matrix was soaked in 1 M nitric acid at 50 °C for 24 h, followed by an aqueous wash to remove nitric acid and a subsequent wash with acetone to replace water. The matrix was then dried at 50 °C in vacuum for 12 h. The surface-silylated matrix was prepared by soaking a surface-hydroxylated matrix in TMCS at room temperature for 6 h, followed by a wash with *n*-hexane and acetone in sequence, and then dried at 120 °C in air for 1 h. FTIR and water contact angle measurements were used to characterize the functionalized pore surfaces. All the FTIR spectra were normalized to the Si—O—Si peak around 1032–1020 cm^{-1}, which was the highest peak in the spectra. Static water contact angle measurements were performed using an automated contact angle goniometer (ramé-hart Model 290, ramé-hart instrument co., Succasunna, NJ). A water droplet (volume = 15 µL) was dropped onto the top surface of the nanoporous matrix. An image of the droplet sitting on top of the surface was taken by the camera of the instrument, and the contact angle at the water/solid interface was calculated by the included software. Toluene adsorption–desorption isotherms of the three types of matrices were measured using EP.

Synthesis of Hybrid Nanocomposites via Polymer Filling: The nanoporous matrix with a spin-coated PS thin film on top was heated at 300 °C in nitrogen for a desired amount of time. The fill level was characterized by XRR and DP-XPS as described previously.[8a,31] A

toluene rinse was employed to remove the excess polymer on top of the matrix after filling for $M_w \leq 426$ kDa, while an extra oxygen plasma exposure and subsequent toluene rinse was required for $M_w > 426$ kDa. Completion of the excess polymer removal was verified by XRR and DP-XPS.

Fabrication and Fracture Energy Measurement of DCB Specimens: On top of the nanocomposite film, sputtering of 25 nm titanium and subsequent evaporation of 125 nm aluminum was conducted to produce adhesion layers. A 50×50 mm square silicon coupon was bonded onto the aluminum layer using an epoxy adhesive (EPO-TEK 353ND, Epoxy Technology, MA). The resultant sample was diced into DCB specimens with a width of 5 mm, a total thickness of 1.46 mm, and a length of 50 mm. Fracture tests of the DCB specimens were conducted on a micromechanical test system (DTS Delaminator Test System, DTS Company, CA) (Figure S1, Supporting Information). The specimen was loaded in tension at a displacement rate of 1 μm s^{-1} to produce stable, cohesive crack growth inside the nanocomposite, then it was unloaded. The load–displacement curve was measured during the fracture test. The cohesive fracture energy (G_c) of the nanocomposites was calculated using the following equation[32]

$$G_c = \frac{12 P_c^2 l^2}{B^2 E' h^3}\left(1 + 0.64 \frac{h}{l}\right)^2 \quad (12)$$

where P_c is the critical load at which crack growth occurs, l is the crack length, E' is the plain strain elastic modulus, B is the width of the specimen, and h is the thickness of the specimen. The fracture surfaces were characterized by DP-XPS to confirm that the crack was cohesive.

Measurement of the Glass Transition Temperatures (Tg) of the Confined Polymers: Flash-DSC) (Mettler Toledo, Flash DSC 1) was used to measure the T_g of the polymers confined in the nanoporous matrix. Nanocomposite sample powders were obtained by scraping the thin films off the silicon substrate. A hair tool was used to directly place as-prepared nanocomposite sample powders or bulk PS powders (≈ng) atop flash-DSC chip sensors under an optical microscope. The surface of a flash-DSC chip sensor consisted of silicon nitride/oxide membranes. During measurement, the heat flow curves of samples were obtained by heating from −60 to 200 °C at a rate of 8000 °C s^{-1}. T_g values were subsequently determined at half-devitrification on heating curves. Two separate measurements were performed for each type of sample.

Supporting Information

Supporting Information is available from the Wiley Online Library or from the author.

Acknowledgements

Conflict of Interest

The authors declare no conflict of interest.

[1] a) L. Li, J. Chen, W. Deng, C. Zhang, Y. Sha, Z. Cheng, G. Xue, D. Zhou, *J. Phys. Chem. B* **2015**, *119*, 5047; b) L. Li, D. Zhou, D. Huang, G. Xue, *Macromolecules* **2013**, *47*, 297.

[2] C. Shao, S. Keten, *Sci. Rep.* **2015**, *5*, 16452.

[3] a) N. Jouault, P. Vallat, F. Dalmas, S. r. Said, J. Jestin, F. o. Boué, *Macromolecules* **2009**, *42*, 2031; b) Z. Y. Zhu, T. Thompson, S. Q. Wang, E. D. von Meerwall, A. Halasa, *Macromolecules* **2005**, *38*, 8816; c) H. Montes, F. Lequeux, J. Berriot, *Macromolecules* **2003**, *36*, 8107; d) X. Chen, M. J. Sobkowicz, *Rheol. Acta* **2015**, *54*, 847.

[4] a) D. M. Sussman, W. S. Tung, K. I. Winey, K. S. Schweizer, R. A. Riggleman, *Macromolecules* **2014**, *47*, 6462; b) J. Martin, M. Krutyeva, M. Monkenbusch, A. Arbe, J. Allgaier, A. Radulescu, P. Falus, J. Maiz, C. Mijangos, J. Colmenero, D. Richter, *Phys. Rev. Lett.* **2010**, *104*, 197801.

[5] A.-C. Shi, B. Li, *Soft Matter* **2013**, *9*, 1398.

[6] S. Askar, T. Wei, A. W. Tan, J. M. Torkelson, *J. Chem. Phys.* **2017**, *146*, 203323.

[7] K. Shin, S. Obukhov, J. T. Chen, J. Huh, Y. Hwang, S. Mok, P. Dobriyal, P. Thiyagarajan, T. P. Russell, *Nat. Mater.* **2007**, *6*, 961.

[8] a) S. G. Isaacson, K. Lionti, W. Volksen, T. P. Magbitang, Y. Matsuda, R. H. Dauskardt, G. Dubois, *Nat. Mater.* **2016**, *15*, 294; b) S. G. Isaacson, J. I. Fostvedt, H. Koerner, J. W. Baur, K. Lionti, W. Volksen, G. Dubois, R. H. Dauskardt, *Nano Lett.* **2017**, *17*, 7040; c) S. G. Isaacson, Y. Matsuda, K. Lionti, T. Frot, W. Volksen, R. H. Dauskardt, G. Dubois, *ACS Appl. Mater. Interfaces* **2018**, *10*, 27549.

[9] P. G. de Gennes, *Scaling Concepts in Polymer Physics*, Cornell University Press, Ithaca, NY **1979**.

[10] W. Volksen, T. P. Magbitang, R. D. Miller, S. Purushothaman, S. A. Cohen, H. Nakagawa, Y. Nobe, T. Kokubo, G. J. M. Dubois, *J. Electrochem. Soc.* **2011**, *158*, G155.

[11] R. K. Iler, *The Chemistry of Silica: Solubility, Polymerization, Colloid and Surface Properties, and Biochemistry*, John Wiley & Sons, Inc., New York, NY **1979**.

[12] X. S. Zhao, G. Q. Lu, *J. Phys. Chem. B* **1998**, *102*, 1556.

[13] a) P. H. T. Ngamou, J. P. Overbeek, R. Kreiter, H. M. van Veen, J. F. Vente, I. M. Wienk, P. F. Cuperus, M. Creatore, *J. Mater. Chem. A* **2013**, *1*, 5567; b) L. Y. Cui, G. Dubois, R. H. Dauskardt, *ACS Appl. Mater. Interfaces* **2016**, *8*, 1309.

[14] S. Saliba, P. Ruch, W. Volksen, T. P. Magbitang, G. Dubois, B. Michel, *Microporous Mesoporous Mater.* **2016**, *226*, 221.

[15] M. S. Nadiye-Tabbiruka, *Colloid Polym. Sci.* **2003**, *281*, 36.

[16] a) J. Abelard, A. R. Wilmsmeyer, A. C. Edwards, W. O. Gordon, E. M. Durke, C. J. Karwacki, D. Troya, J. R. Morris, *J. Phys. Chem. C* **2016**, *120*, 13024; b) M. L. Hair, W. Hertl, *J. Phys. Chem.* **1969**, *73*, 4269.

[17] A. V. Kiselev, *Q. Rev., Chem. Soc.* **1961**, *15*, 99.

[18] a) E. W. Washburn, *Phys. Rev.* **1921**, *17*, 273; b) R. Lucas, *Kolloid-Z.* **1918**, *23*, 15.

[19] Y. Yao, S. Alexandris, F. Henrich, G. Auernhammer, M. Steinhart, H. J. Butt, G. Floudas, *J. Chem. Phys.* **2017**, *146*, 203320.

[20] a) M. P. Goertz, J. E. Houston, X. Y. Zhu, *Langmuir* **2007**, *23*, 5491; b) J. Bowen, D. Cheneler, M. J. Adams, *Colloids Surf. A* **2013**, *418*, 112.

**ADVANCED
SCIENCE NEWS**

www.advancedsciencenews.com

**ADVANCED
FUNCTIONAL
MATERIALS**

www.afm-journal.de

[21] N. K. Lee, J. Farago, H. Meyer, J. P. Wittmer, J. Baschnagel, S. P. Obukhov, A. Johner, *EPL* **2011**, *93*, 48002.

[22] W. S. Tung, R. J. Composto, R. A. Riggleman, K. I. Winey, *Macromolecules* **2015**, *48*, 2324.

[23] P. Claudy, J. M. Letoffe, Y. Camberlain, J. P. Pascault, *Polym. Bull.* **1983**, *9*, 208.

[24] S. Alexandris, P. Papadopoulos, G. Sakellariou, M. Steinhart, H.-J. Butt, G. Floudas, *Macromolecules* **2016**, *49*, 7400.

[25] H. Leese, V. Bhurtun, K. P. Lee, D. Mattia, *Colloids Surf., A* **2013**, *420*, 53.

[26] E. J. Kramer, *Adv. Polym. Sci.* **1983**, *52–53*, 1.

[27] a) L. T. Drzal, M. Madhukar, M. C. Waterbury, *Compos. Struct.* **1994**, *27*, 65; b) J. Homeny, W. L. Vaughn, M. K. Ferber, *J. Am. Ceram. Soc.* **1990**, *73*, 394; c) B. M. Gallant, X. W. Gu, D. Z. Chen, J. R. Greer, N. S. Lewis, *ACS Nano* **2015**, *9*, 5143; d) T. Ozkan, Q. Chen, I. Chasiotis, *Compos. Sci. Technol.* **2012**, *72*, 965; e) C. J. Cho, L. O'Leary, N. S. Lewis, J. R. Greer, *Nano Lett.* **2012**, *12*, 3296.

[28] A. Ghorbal, S. Bistac, M. Schmitt, *J. Polym. Sci., Part B: Polym. Phys.* **2006**, *44*, 2449.

[29] a) S. Zhandarov, E. Mader, *Compos. Sci. Technol.* **2005**, *65*, 149; b) P. S. Chua, M. R. Piggott, *Compos. Sci. Technol.* **1985**, *22*, 185; c) M. R. Piggott, P. S. Chua, *Ind. Eng. Chem. Res.* **1987**, *26*, 672.

[30] M. Sambasivam, A. Klein, L. H. Sperling, *Macromolecules* **1995**, *28*, 152.

[31] T. Frot, W. Volksen, S. Purushothaman, R. L. Bruce, T. Magbitang, D. C. Miller, V. R. Deline, G. Dubois, *Adv. Funct. Mater.* **2012**, *22*, 3043.

[32] M. Giachino, G. Dubois, R. H. Dauskardt, *ACS Appl. Mater. Interfaces* **2013**, *5*, 9891.

1903132 (9 of 9)

Using Unentangled Oligomers To Toughen Materials

Scott G. Isaacson,[†] Yusuke Matsuda,[†] Krystelle Lionti,[‡] Theo Frot,[‡] Willi Volksen,[‡] Reinhold H. Dauskardt,[*,†] and Geraud Dubois[*,†,§]

[†]Department of Materials Science and Engineering, Stanford University, 496 Lomita Mall, Stanford, California 94305, United States

[‡]Hybrid Polymeric Materials and [§]Science to Solutions, IBM Almaden Research Center, 650 Harry Road, San Jose, California 95120-6099, United States

Ⓢ *Supporting Information*

ABSTRACT: Entanglements between polymer chains are responsible for the strength and toughness of polymeric materials. When the chains are too short to form entanglements, the polymer becomes weak and brittle. Here we show that molecular bridging of oligomers in molecular-scale confinement can dramatically toughen materials even when intermolecular entanglements are completely absent. We describe the fabrication of nanocomposite materials that confine oligomer chains to molecular-scale dimensions and demonstrate that partially confined unentangled oligomers can toughen materials far beyond rule-of-mixtures estimates. We also characterize how partially confined oligomers affect the kinetics of nanocomposite cracking in moist environments and show that the presence of a backfilled oligomeric phase within a nanoporous organosilicate matrix leads to atomistic crack path meandering in which the failure path is preferentially located within the matrix phase.

KEYWORDS: *polymer confinement, nanocomposites, fracture toughness, porous materials, polymer entanglements*
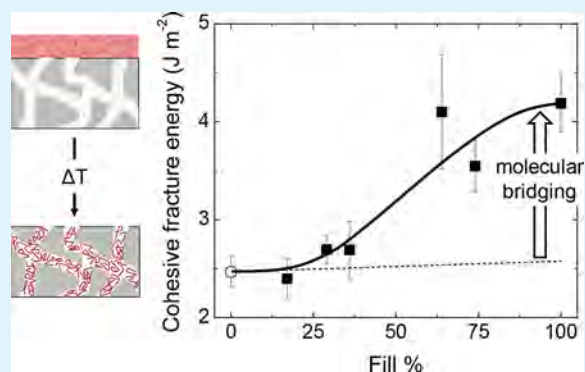
Molecular-scale confinement of polymers has generated intense interest because of its ability to induce changes in many polymer properties, including altered molecular dynamics,[1−6] changes in scaling behavior,[7] and reduction of interchain entanglements.[7−9] This last property of polymer confinement has important implications for the fracture of confined polymers because entanglements enable mechanisms that give high-molecular-mass bulk polymers their high toughness.[10] We have recently demonstrated the effects of polymer confinement on the fracture properties of nanocomposite materials, showing that high-molecular-mass polymers confined at molecular length scales dissipate energy through a confinement-induced molecular bridging mechanism.[11,12] Although confinement-induced bridging substantially increased the toughness in these materials, the magnitude of their fracture energy was far lower than that of bulk polymers because of the reduction in entanglements[7−9] and suppression of traditional polymer toughening mechanisms such as crazing.[10] We now turn our attention to the toughening behavior of low-molecular-mass oligomers that are confined at molecular length scales. Such molecules are of particular interest because they are large enough to undergo molecular bridging but are too short to form intermolecular entanglements. Because of their lack of strong interactions between chains, these oligomers have low fracture toughness values in the bulk.[13] We show that their fracture toughness can

increase substantially in molecular-scale confinement, increasing the fracture energy of nanocomposites by up to 70%.

To experimentally generate molecular-scale confinement of oligomer chains, we fabricated hybrid nanocomposites composed of an oligomeric phase confined within a nanoporous organosilicate matrix. The matrix was obtained by the spin casting and subsequent thermal curing of a porogen-containing ethylene oxycarbosilane/methylsilsesquioxane (Et-OCS/MSSQ) sol−gel formulation atop a silicon wafer coated with a dense silicon carbon nitride (SiCN) adhesion layer. This process created matrix films approximately 600 nm in thickness with a porosity of 40%. These materials are typically used as low-*k* dielectrics for advanced applications in the microelectronics industry.[14−18] The porosity was composed of a random interconnected network of approximately cylindrical pores. Ellipsometric porosimetry was used to measure the pore-size distribution, which revealed a range of pore diameters between 1.2 and 3.5 nm, with a mean pore diameter of 2.6 nm (Figure 1a). This pore size was substantially smaller than that in our previous work[11,12] in order to provide molecular-scale confinement of relatively short oligomer chains. The properties of the unfilled matrix are summarized in Table 1.
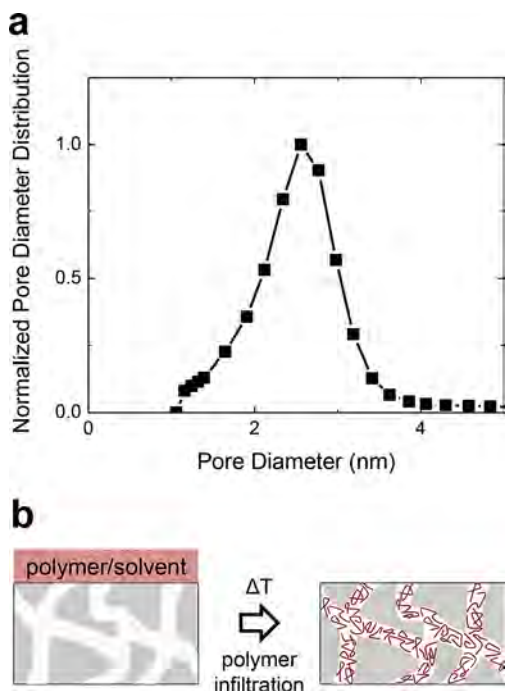
Figure 1. (a) Pore-size distribution of the unfilled organosilicate matrix using methods described elsewhere.[33] The distribution was calculated by applying the Kelvin equation to a toluene adsorption isotherm. (b) Schematic illustration of the nanocomposite structure and polymer-filling process.

Table 1. Material Properties of the Unfilled Organosilicate Matrix Used To Confine Unentangled Oligomer Chains

density, ρ (g cm^{-3})	pore diameter (nm)	porosity (vol %)	refractive index
0.895	2.6	40	1.273

To fill the nanoporous matrix, an oligomer solution was spin-cast onto the matrix and heated at 150 °C on a hot plate for at least 15 min (Figure 1b). This allowed the oligomer chains to infiltrate the porosity of the matrix and resulted in a hybrid nanocomposite material containing oligomer molecules. By controlling the thickness of the initial spin-cast oligomer layer, the fill level could be controlled. The film thickness and refractive index were measured using a Filmetrics F20 spectral reflectometer. The fill level, fill uniformity, and film density were characterized with spectral X-ray reflectivity (XRR) measurements using a diffractometer (X'Pert PRO MRD, PANalytical) with a ceramic X-ray tube (wavelength = 0.154 nm) and a high-resolution horizontal goniometer (reproducibility ±0.0001°). Importantly, this characterization demonstrated that it was possible to partially fill the nanoporous matrix with oligomer chains while maintaining a homogeneous distribution of oligomers throughout the thickness of the film. Homogeneous filling of the nanoporous matrix and the presence of a dense SiCN adhesion layer are both essential requirements for cohesive crack propagation through the nanocomposite layer and accurate measurement of the nanocomposite fracture toughness.

The degree of confinement experienced by the oligomer chains is strongly influenced by the molecular mass (M_w) and pore diameter (Figure 2). For a nanoporous matrix with pore diameters between $d_{pore,min}$ = 1.2 nm and $d_{pore,max}$ = 3.5 nm, polystyrene chains with $M_w \leq 700$ g mol^{-1} are unconfined
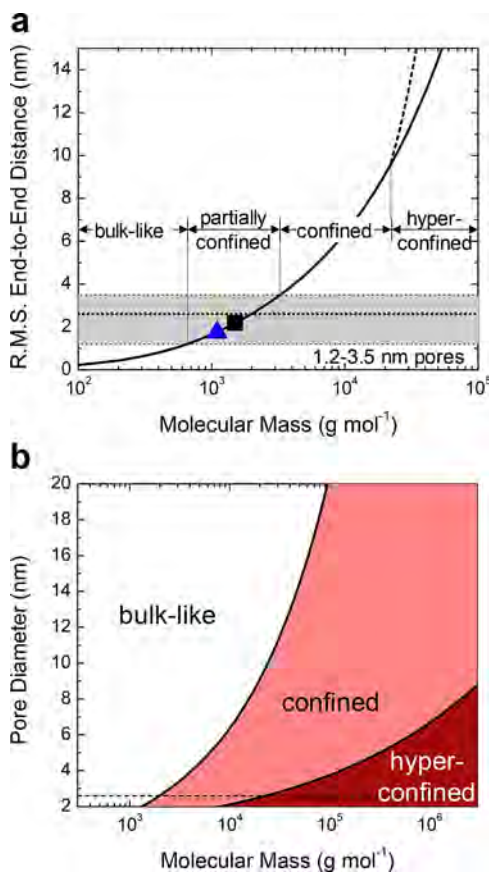

Figure 2. Molecular confinement of polystyrene in cylindrical pores. (a) Polystyrene (black square) with M_w = 1500 g mol^{-1} has an rms end-to-end distance R_{ee} of 2.2 nm and PMMA (blue triangle) with M_w = 1100 g mol^{-1} has R_{ee} of 1.7 nm, meaning that only some chains meet the confinement condition of $R_{ee} > d_{pore}$. (b) Molecular mass onsets of the confined and hyperconfined regimes for polystyrene chains depend strongly on the pore diameter. The average pore diameter of the nanoporous organosilicate matrix used in this study is shown as a dashed line.

[root-mean-square (rms) end-to-end distance $R_{ee} \leq d_{pore,min}$]. Polystyrene molecules with 700 g mol^{-1} < M_w < 3300 g mol^{-1} are partially confined, possessing molecular sizes that are larger than some of the pores ($d_{pore,min} < R_{ee} < d_{pore,max}$). Chains with $M_w \geq 3300$ g mol^{-1} are subjected to full confinement within the pore structure ($R_{ee} > d_{pore,max}$). The dependence of R_{ee} on M_w for polystyrene is shown in Figure 2a. Remarkably, even under confinement, polystyrene chains in 2.6 nm pores retain their bulk end-to-end distances up to a molecular mass of approximately 23000 g mol^{-1} (confined size of 10 nm) and only adopt more extended conformations at higher molecular masses (hyperconfined regime; Figure 2).[7,11] The value of R_{ee} for 1100 g mol^{-1} poly(methyl methacrylate) (PMMA) is shown in Figure 2a, and the onsets of the partially confined, confined, and hyperconfined regimes for confined PMMA in 2.6 nm pores are shown in Figure S1. The wormlike chain model[19] was used to calculate R_{ee} for both PMMA and polystyrene oligomers in order to account for the non-Gaussian nature of low-M_w chains. The oligomer end-to-end distance was selected as the appropriate confinement length scale because this parameter best captures the full spatial extent of the chains that is available for interactions with the

surrounding pore walls while remaining straightforward to calculate from established models.[19]

By using a nanoporous matrix with such small pores (Figure 2b), it is possible to study chains that are confined ($R_{ee} > d_{pore}$) but are also well below the critical entanglement molecular mass, M_c ($M_w \ll M_c$). Oligomers with $M_w \ll M_c$ cannot form effective entanglements between chains and cannot be effectively toughened by common mechanisms such as crazing.[10,20] Such oligomeric solids are held together primarily by relatively weak intermolecular bonds instead of entanglements and have low fracture toughness values.[13]

Double-cantilever beam fracture mechanics specimens (Figure S2) were used to measure the cohesive fracture energy, G_c, of the hybrid nanocomposite films (Figure 3a)
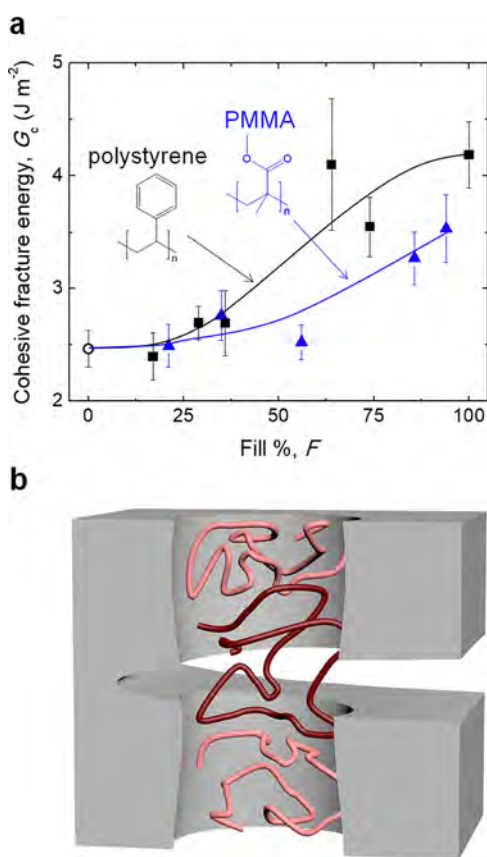

Figure 3. (a) Cohesive fracture energy of hybrid nanocomposites as a function of the oligomer filling percentage. Confined polystyrene (black squares) has a slightly larger toughening effect than PMMA (blue triangles). (b) Idealized representation of a crack front propagating through a nanoporous organosilicate containing confined oligomer chains. The central, dark-red chain is participating in the molecular bridging mechanism by bridging the separating fracture surfaces and pulling out from the pore structure. The adjacent pink chains are not entangled with surrounding oligomers and are unaffected by the advancing crack.

filled with polystyrene with $M_w = 1500$ g mol^{-1}. This molecular mass is well below the critical entanglement molecular mass of polystyrene (31200 g mol^{-1}),[21] ensuring that the oligomer phase lacked any entanglements. The cohesive fracture energy of the nanocomposites was measured as a function of the oligomer filling percentage, F, which is defined as the volume percentage of the porous network occupied by oligomer chains. A simple (and incorrect) rule-of-mixtures estimate for

the fracture energy would predict only very small increases in G_c with increasing F due to the lack of crazing in unentangled polystyrene. At $F = 0$, the unfilled nanoporous matrix had a relatively low fracture energy of 2.5 J m^{-2} that is characteristic of nanoporous glasses.[22] As F was increased, the fracture energy rose significantly beyond the rule-of-mixtures estimate, reaching a maximum value of 4.2 J m^{-2} when fully filled with polystyrene. Such increases in G_c are remarkable given the fragile nature of bulk polystyrene with the same M_w, which has a fracture energy of 0.25 J m^{-2}.[13] These results show that the traditional energy dissipation mechanisms of low-M_w polymer fracture cannot be responsible for the increased fracture energy in these materials.

Instead, the significant toughening achieved with unentangled oligomers is due to molecular bridging of the oligomer chains.[11,12] In this mechanism, oligomer molecules that are intercepted by an advancing crack front bridge the separating fracture surfaces. As the crack propagates, the chains pull out from the pore structure and elongate, dissipating energy in the process (Figure 3b). Previous studies have used molecular-scale analogues of well-known fiber bridging models to demonstrate that this mechanism is consistent with the scaling of polymer chains in cylindrical confinement and provides reasonable estimates of the polymer−matrix interaction strength and the ultimate tensile strength of individual polymer chains.[11] The results of the present study show that the molecular bridging mechanism can be induced by relatively weak molecular-scale confinement of oligomer chains and can toughen materials even in the absence of molecular entanglements. The substantial increases in G_c observed for these nanocomposites demonstrate that the molecular bridging mechanism can be leveraged to induce significant toughening with low-M_w polymers that have very low toughness on their own but provide significant toughening when confined at molecular length scales.

Recent results have shown that similar materials systems such as liquids confined within a solid matrix can exhibit increased stiffness and dynamic energy absorption.[23] Such an effect has been considered as an alternative explanation for the increases in the fracture energy demonstrated in this work. However, this mechanism relies on large deformations of liquid inclusions and the surrounding matrix. In this work, the organosilicate matrix into which the polystyrene and PMMA oligomers are infiltrated is a highly porous glass that is brittle ($G_c = 2.5$ J m^{-2}) and stiff relative to the oligomer second phase. Such properties render the organosilicate matrix unable to tolerate significant strain (relative to the confined oligomers) before fracture. This characteristic of the materials system suggests that the energy dissipation mechanisms related to confined liquids in a compliant matrix are unlikely to significantly contribute to the observed toughening.

The fracture energy of nanocomposites filled with PMMA with $M_w = 1100$ g mol^{-1} was also measured as a function of F. This molecular mass is well below the critical entanglement molecular mass for PMMA (18400 g mol^{-1}).[21] The PMMA nanocomposites showed a toughening behavior similar to that of nanocomposites filled with polystyrene, with a maximum G_c of 3.5 J m^{-2} (Figure 3a). The difference in the magnitude of the toughening effect between polystyrene and PMMA could be due to differing oligomer−pore interaction strengths, which would change the stress required for pullout and thus the overall fracture energy.[11]

The observed toughening behavior of partially confined polystyrene and PMMA shows that toughening with unentangled oligomer chains is not a phenomenon that is unique to polystyrene but instead extends to other polymers as well. These results suggest an alternative route to improving the toughness of nanocomposites and devices containing unconfined low-molecular-mass polymers. Instead of increasing the molecular mass of the polymer phase to increase toughness, one could alternatively reduce the confinement length scale (e.g., pore diameter) and take advantage of the confinement-induced molecular bridging mechanism (Figure 2b).

Thus far, we have focused on characterizing the critical fracture behavior of hybrid nanocomposites containing oligomers in molecular-scale confinement. We now turn our attention to how oligomer confinement affects the kinetics of crack propagation in nanocomposites. In silica-based materials, water vapor from the surrounding environment can react with strained bonds at the crack tip to induce time-dependent crack growth at values of the strain energy release rate, G, that are below the value required for critical fracture, G_c.[24] The time-dependent crack propagation was characterized by measuring the crack growth rates as a function of the applied strain energy release rate, G. We first measured the crack growth rates of the unfilled matrix in environments with different moisture levels: 20% relative humidity (RH), 80% RH, and in a fully aqueous environment (Figure 4). The unfilled matrix exhibited time-dependent crack growth below G_c and reached a crack growth threshold, G_{th}, below which crack growth was presumed to be dormant. The measured crack growth curves shifted to lower values of G with increasing moisture content, as indicated by a decrease in the values of G_{th} from ~1.5 J m^{-2} in a 20% RH environment to ~1.0 J m^{-2} in water. The observed behavior indicates the high sensitivity of nanoporous glass films to moisture-assisted cracking, similar to other silica-based materials.[24,25]

We then measured the crack growth rates in nano-composites filled with partially confined PMMA (M_w = 1100 g mol^{-1}) and polystyrene (M_w = 1500 g mol^{-1}) as a function of the applied G (Figure 4b,c). F was 94% for PMMA and 100% for polystyrene. The filled hybrid nanocomposite films similarly exhibited time-dependent crack growth in moist environments and a decrease in G_{th} with increasing moisture content (with the exception of PMMA nanocomposites in water; Figure 4b). The values of G_{th} in different environments were higher than the corresponding G_{th} values of the unfilled film, however, indicating that the addition of partially confined oligomers still provides protection from moisture-assisted cracking.

Such increases in G_{th} are mostly due to the mechanical shielding of the crack tip by the confinement-induced molecular bridging of the filled oligomers. G_{th} for the filled hybrid nanocomposite films may be expressed as the sum of the contributions from the organosilicate matrix and the oligomer phase[26]

$$G_{th} = G_{th}^{OSG} + G_{th}^{polymer} \qquad (1)$$

where G_{th}^{OSG} and $G_{th}^{polymer}$ represent G_{th} for the organosilicate glass and partially confined oligomers, respectively. While G_{th}^{OSG} is highly sensitive to moisture and decreases with increasing moisture content,[27] $G_{th}^{polymer}$ is largely insensitive to moisture[28−30] and contributes to the elevated values of G_{th} in filled films.
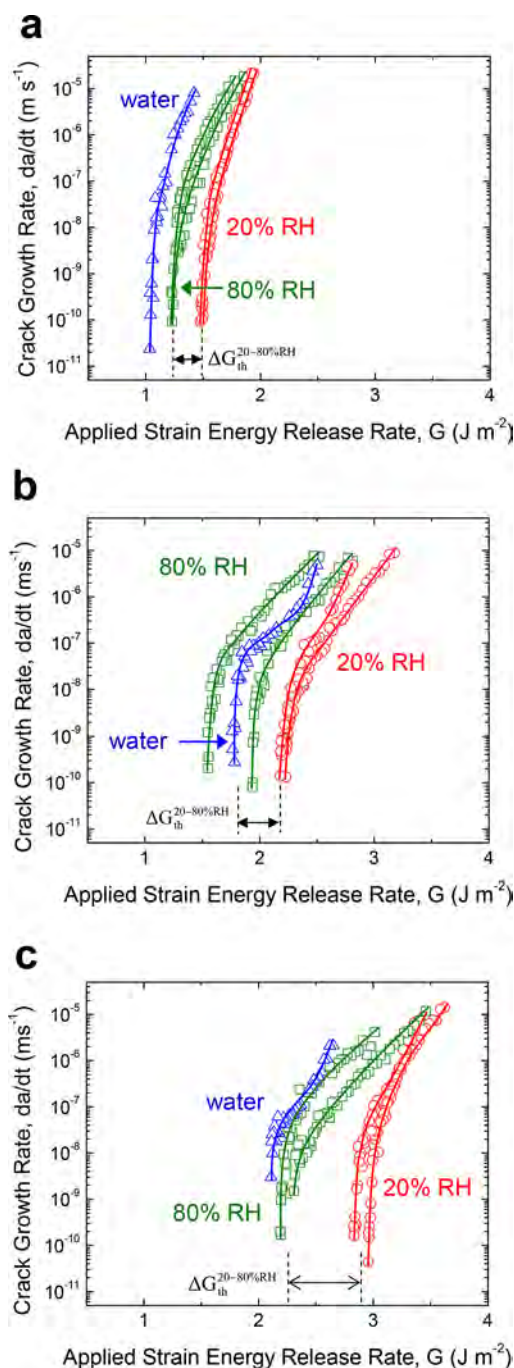
Figure 4. Crack growth rate of hybrid nanocomposites as a function of the applied strain energy release rate: (a) no fill ($F = 0\%$); (b) filled with PMMA ($F = 94\%$); (c) filled with polystyrene ($F = 100\%$).

Although the values of G_{th} for the hybrid nanocomposite films were increased by the partially confined oligomers, the nanocomposites became more sensitive to moisture-assisted cracking when filled with an oligomeric phase. This is evidenced by an increase in the difference between the G_{th} values at different humidity levels. This difference is referred to as ΔG_{th} and is a measure of the sensitivity of materials to moisture-assisted cracking. The values of ΔG_{th} between 20% and 80% RH increased from 0.30 J m^{-2} for the unfilled films to 0.45 J m^{-2} for those filled with PMMA and to 0.65 J m^{-2} for those filled with polystyrene. Because $G_{th}^{polymer}$ is assumed to be

independent of changes in relative humidity, ΔG_{th} may be expressed[26,31] as

$$\Delta G_{th} = N_{Si-O-Si} kT \ln\left(\frac{P_{H_2O}''}{P_{H_2O}'}\right) \tag{2}$$

where k is the Boltzmann constant, T is the temperature in Kelvin, $N_{Si-O-Si}$ is the number of Si−O−Si bonds ruptured per unit area, and P_{H_2O} is the partial pressure of water (with superscripts representing the environments with different moisture contents). ΔG_{th} is primarily dependent on $N_{Si-O-Si}$, which depends on the crack path at an atomistic scale. For a planar crack, the number of ruptured Si−O−Si bonds would be a fixed value. However, if the crack were to deviate from a planar path and meander in three dimensions, the value of $N_{Si-O-Si}$ could change.

Table 2 summarizes the measured values of ΔG_{th} with different partially confined oligomers as well as the

Table 2. Shifts of G_{th} between 20% and 80% RH for Hybrid Nanocomposites with Different Oligomer Fillers

filling oligomer	$\Delta G_{th}^{20-80\% \ RH}$	$N_{Si-O-Si}$
no fill	0.30	73
PMMA	0.45	109
polystyrene	0.65	158

corresponding values of $N_{Si-O-Si}$ calculated using eq 2. While it is not currently feasible to characterize the atomistic crack path experimentally, the path can be inferred by comparing the $N_{Si-O-Si}$ values calculated from eq 2 with those estimated from a planar crack model. For a planar crack, $N_{Si-O-Si}$ only depends on the volume density of the Si−O−Si bonds:

$$N_{Si-O-Si} = \rho_{Si-O-Si}^{2/3} \tag{3}$$

Using eq 3, we estimate the value of $N_{Si-O-Si}$ for a planar crack to be approximately 7 nm^{-2}. The values of $N_{Si-O-Si}$ calculated from eq 2 are significantly higher than those in the case of a planar crack, indicating that the crack path meanders in three dimensions to increase the number of intercepted Si−O−Si bonds.[31] In moist environments, the Si−O bond energy is reduced from 800 to ∼139 kJ mol^{-1} in the presence of water molecules,[32] which facilitates atomistic crack path meandering within the organosilicate phase. Furthermore, filling the organosilicate matrix with partially confined oligomers increases $N_{Si-O-Si}$, indicating increased crack path meandering in which the crack preferentially propagates through the organosilicate phase. Note that, although crack path meandering has been demonstrated in other materials,[31] the magnitude of the calculated increase in $N_{Si-O-Si}$ over a planar crack is surprising. It is possible that in this materials system the value of $G_{th}^{polymer}$ is reduced at high RH. This could occur if moisture absorbed into the oligomer phase reduces the interfacial sliding stress between the oligomer chains and pore walls, which would result in a larger value of ΔG_{th} and an overestimate of $N_{Si-O-Si}$.

This study demonstrates that unentangled oligomer chains can toughen nanocomposites far beyond rule-of-mixtures estimates through a confinement-induced molecular bridging mechanism. When these oligomers are infiltrated into an organosilicate matrix, they improve its resistance to moisture-assisted cracking and induce crack path meandering in which

the failure path is preferentially located within the matrix phase. These insights into the fracture behavior of partially confined unentangled oligomers will aid in the design of nanocomposites and nanoscale devices that contain low-molecular-mass polymers.

■ ASSOCIATED CONTENT

ⓢ Supporting Information

The Supporting Information is available free of charge on the ACS Publications website at DOI: 10.1021/acsami.8b03050.

Supplementary Figures S1 and S2 and methods (PDF)

■ AUTHOR INFORMATION

Corresponding Authors

*E-mail: dauskardt@stanford.edu.
*E-mail: gdubois@us.ibm.com.

ORCID Ⓘ

Reinhold H. Dauskardt: 0000-0003-3989-362X

Author Contributions

The manuscript was written through contributions of all authors. All authors have given approval to the final version of the manuscript.

Notes

The authors declare no competing financial interest.

■ ABBREVIATIONS

Et-OCS/MSSQ = ethylene oxycarbosilane/methylsilsesquioxane
PMMA = poly(methyl methacrylate)
SiCN = silicon carbon nitride
XRR = X-ray reflectivity

■ REFERENCES

(1) Rittigstein, P.; Priestley, R. D.; Broadbelt, L. J.; Torkelson, J. M. Model Polymer Nanocomposites Provide an Understanding of Confinement Effects in Real Nanocomposites. *Nat. Mater.* **2007**, *6*, 278−282.

(2) Krutyeva, M.; Wischnewski, A.; Richter, D. Polymer Dynamics in Nanoconfinement: Interfaces and Interphases. *EPJ Web Conf.* **2015**, *83*, 02009.

(3) Romo-Uribe, A.; Cardoso, J. Viscoelasticity and Dynamics of Confined Polyelectrolyte/Layered Silicate Nanocomposites: The Influence of Intercalation and Exfoliation. *Macromol. Chem. Phys.* **2018**, *219*, 1700448.

(4) Krishnamoorti, R.; Vaia, R. A.; Giannelis, E. P. Structure and Dynamics of Polymer-Layered Silicate Nanocomposites. *Chem. Mater.* **1996**, *8*, 1728−1734.

(5) Fatkullin, N.; Kimmich, R.; Fischer, E.; Mattea, C.; Beginn, U.; Kroutieva, M. The Confined-to-Bulk Dynamics Transition of Polymer Melts in Nanoscopic Pores of Solid Matrices with Varying Pore Diameter. *New J. Phys.* **2004**, *6*, 46.

(6) Schönhals, A.; Goering, H.; Schick, C.; Frick, B.; Zorn, R. Glassy Dynamics of Polymers Confined to Nanoporous Glasses Revealed by Relaxational and Scattering Experiments. *Eur. Phys. J. E: Soft Matter Biol. Phys.* **2003**, *12*, 173−178.

(7) De Gennes, P.-G. *Scaling Concepts in Polymer Physics*; Cornell University Press: Ithaca, NY, 1979.

(8) Rowland, H.; King, W.; Pethica, J.; Cross, G. Molecular Confinement Accelerates Deformation of Entangled Polymers During Squeeze Flow. *Science* **2008**, *322*, 720−724.

(9) Si, L.; Massa, M. V.; Dalnoki-Veress, K.; Brown, H. R.; Jones, R. A. L. Chain Entanglement in Thin Freestanding Polymer Films. *Phys. Rev. Lett.* **2005**, *94*, 127801.

(10) Kramer, E. Microscopic and Molecular Fundamentals of Crazing. In *Crazing in Polymers*; Kausch, H. H., Ed.; Springer-Verlag: Berlin/Heidelberg, 1983; pp 1−56.

(11) Isaacson, S. G.; Lionti, K.; Volksen, W.; Magbitang, T. P.; Matsuda, Y.; Dauskardt, R. H.; Dubois, G. Fundamental Limits of Material Toughening in Molecularly Confined Polymers. *Nat. Mater.* **2016**, *15*, 294−298.

(12) Isaacson, S. G.; Fostvedt, J. I.; Koerner, H.; Baur, J. W.; Lionti, K.; Volksen, W.; Dubois, G.; Dauskardt, R. H. Synthesis of Polyimides in Molecular-Scale Confinement for Low Density Hybrid Nano-composites. *Nano Lett.* **2017**, *17*, 7040−7044.

(13) Robertson, R. E. The Fracture Energy of Low Molecular Weight Fractions of Polystyrene. In *Toughness and Brittleness of Plastics*; Deanin, R. D.; Crugnola, A. M., Eds.; American Chemical Society: Washington, DC, 1976; pp 89−96.

(14) Volksen, W.; Magbitang, T. P.; Miller, R. D.; Purushothaman, S.; Cohen, S.A.; Nakagawa, H.; Nobe, Y.; Kokubo, T.; Dubois, G. J. M. A Manufacturing Grade, Porous Oxycarbosilane Spin-on Dielectric Candidate with K ≤ 2.0. *J. Electrochem. Soc.* **2011**, *158*, G155−G161.

(15) Volksen, W.; Purushothaman, S.; Darnon, M.; Lofaro, M. F.; Cohen, S. A.; Doyle, J. P.; Fuller, N.; Magbitang, T. P.; Rice, P. M.; Krupp, L. E.; Nakagawa, H.; Nobe, Y.; Kokubo, T.; Dubois, G. J. M. Integration of a Manufacturing Grade, k = 2.0 Spin-on Material in a Single Damascene Structure. *ECS J. Solid State Sci. Technol.* **2012**, *1*, N85−N90.

(16) Volksen, W.; Miller, R.; Dubois, G. Low Dielectric Constant Materials. *Chem. Rev.* **2010**, *110*, 56−110.

(17) Volksen, W.; Lionti, K.; Magbitang, T.; Dubois, G. Hybrid Low Dielectric Constant Thin Films for Microelectronics. *Scr. Mater.* **2014**, *74*, 19−24.

(18) Lionti, K.; Volksen, W.; Magbitang, T.; Darnon, M.; Dubois, G. Toward Successful Integration of Porous Low-k Materials: Strategies Addressing Plasma Damage. *ECS J. Solid State Sci. Technol.* **2015**, *4*, N3071−N3083.

(19) Benoit, H.; Doty, P. Light Scattering from Non Gaussian Chains. *J. Phys. Chem.* **1953**, *57*, 958−963.

(20) Donald, A. M.; Kramer, E. J. Effect of Molecular Entanglements on Craze Microstructure in Glassy Polymers. *J. Polym. Sci., Polym. Phys. Ed.* **1982**, *20*, 899−909.

(21) Wool, R. P. Polymer Entanglements. *Macromolecules* **1993**, *26*, 1564−1569.

(22) Maidenberg, D. A.; Volksen, W.; Miller, R. D.; Dauskardt, R. H. Toughening of Nanoporous Glasses Using Porogen Residuals. *Nat. Mater.* **2004**, *3*, 464−469.

(23) Owuor, P. S.; Hiremath, S.; Chipara, A. C.; Vajtai, R.; Lou, J.; Mahapatra, D. R.; Tiwary, C. S.; Ajayan, P. M. Nature Inspired Strategy to Enhance Mechanical Properties via Liquid Reinforcement. *Adv. Mater. Interfaces* **2017**, *4*, 1700240.

(24) Freiman, S. W.; Wiederhorn, S. M.; Mecholsky, J. J., Jr. Environmentally Enhanced Fracture of Glass: A Historical Perspective. *J. Am. Ceram. Soc.* **2009**, *92*, 1371−1382.

(25) Matsuda, Y.; Rathore, J. S.; Interrante, L. V.; Dauskardt, R. H.; Dubois, G. Moisture-Insensitive Polycarbosilane Films with Superior Mechanical Properties. *ACS Appl. Mater. Interfaces* **2012**, *4*, 2659−2663.

(26) Matsuda, Y.; King, S. W.; Bielefeld, J.; Xu, J.; Dauskardt, R. H. Fracture Properties of Hydrogenated Amorphous Silicon Carbide Thin Films. *Acta Mater.* **2012**, *60*, 682−691.

(27) Guyer, E. P.; Patz, M.; Dauskardt, R. H. Fracture of Nanoporous Methyl Silsesquioxane Thin-Film Glasses. *J. Mater. Res.* **2006**, *21*, 882−894.

(28) Marshall, G. P.; Coutts, L. H.; Williams, J. G. Temperature Effects in the Fracture of PMMA. *J. Mater. Sci.* **1974**, *9*, 1409−1419.

(29) Kamer, A.; Larson-Smith, K.; Pingree, L. S. C.; Dauskardt, R. H. Adhesion and Degradation of Hard Coatings on Poly (Methyl Methacrylate) Substrates. *Thin Solid Films* **2011**, *519*, 1907−1913.

(30) Beaumont, P. W. R.; Young, R. J. Failure of Brittle Polymers by Slow Crack Growth. *J. Mater. Sci.* **1975**, *10*, 1334−1342.

(31) Matsuda, Y.; King, S. W.; Oliver, M.; Dauskardt, R. H. Moisture-Assisted Cracking and Atomistic Crack Path Meandering in Oxidized Hydrogenated Amorphous Silicon Carbide Films. *J. Appl. Phys.* **2013**, *113*, 083521.

(32) Wiederhorn, S. M.; Fuller, E. R.; Thomson, R. Micro-mechanisms of Crack Growth in Ceramics and Glasses in Corrosive Environments. *Met. Sci.* **1980**, *14*, 450−458.

(33) Dubois, G.; Volksen, W.; Magbitang, T.; Miller, R. D.; Gage, D. M.; Dauskardt, R. H. Molecular Network Reinforcement of Sol-Gel Glasses. *Adv. Mater.* **2007**, *19*, 3989−3994.